Physica 7D (1983) 181–200
North-Holland Publishing Company

CRISES, SUDDEN CHANGES IN CHAOTIC ATTRACTORS, AND TRANSIENT CHAOS

Celso GREBOGI and Edward OTT
Laboratory for Plasma and Fusion Energy Studies, University of Maryland, College Park, Md. 20742, USA

and

James A. YORKE
Institute for Physical Science and Technology and Department of Mathematics, University of Maryland, College Park, Md. 20742, USA

The occurrence of sudden qualitative changes of chaotic dynamics as a parameter is varied is discussed and illustrated. It is shown that such changes may result from the collision of an unstable periodic orbit and a coexisting chaotic attractor. We call such collisions *crises*. Phenomena associated with crises include sudden changes in the size of chaotic attractors, sudden appearances of chaotic attractors (a possible route to chaos), and sudden destructions of chaotic attractors and their basins. This paper presents examples illustrating that crisis events are prevalent in many circumstances and systems, and that, just past a crisis, certain characteristic statistical behavior (whose type depends on the type of crisis) occurs. In particular the phenomenon of chaotic transients is investigated. The examples discussed illustrate crises in progressively higher dimension and include the one-dimensional quadratic map, the (two-dimensional) Hénon map, systems of ordinary differential equations in three dimensions and a three-dimensional map. In the case of our study of the three-dimensional map a new route to chaos is proposed which is possible only in invertible maps or flows of dimension at least three or four, respectively. Based on the examples presented the following conjecture is proposed: almost all sudden changes in the size of chaotic attractors and almost all sudden destructions or creations of chaotic attractors and their basins are due to crises.

Contents

1. Introduction

The study of attractors and how they change as a parameter of the system is varied is of great interest and has received much attention. Topics in this area include bifurcation theory [1], period-doubling cascades resulting in chaos [2], etc. In this paper we review and discuss some aspects of sudden changes in chaotic attractors which occur as a system parameter is varied. In particular, we discuss certain events which we call *crises* [3]. We define a crisis to be *a collision between a chaotic attractor and a coexisting unstable fixed point or periodic orbit*. In the following four sections we offer examples and discussion illustrating our main points:

(1) crises appear to be the cause of most sudden changes in chaotic dynamics (with the exception of "subductions" to be described later);

(2) such events occur in many circumstances and systems; and

(3) following the occurrence of a crisis, certain

characteristic statistical behavior (which depends on the type of crisis) occurs.

In general, to illustrate the above, the material of this paper consists of a combination of review and interpretation of past work, as well as new research results.

In section 2 we treat the case of the one-dimensional quadratic map. This simple paradigmatic example is used to introduce and distinguish two types of crises, the *boundary crisis* and the *interior crisis*. The former leads to sudden destruction of the chaotic attractor and its basin of attraction, while the latter can cause sudden changes in the size of the chaotic attractor. Section 2 also discusses the associated characteristic statistical behavior occurring for parameter values just past that at which the crisis takes place. In the case of the boundary crisis, for parameter values just past the crisis point, the attractor no longer exists. Nevertheless, typical trajectories initialized in the region formerly occupied by the destroyed attractor appear to move about in this region chaotically, as before the crisis occurred, but only for a finite time after which the orbit rapidly leaves the region (a *chaotic transient*). In the case of an interior crisis, the attractor suddenly increases in size, and we study the dependence of the fraction of time a typical orbit on an attractor of increased size spends in the formerly empty region as a function of closeness of the parameter to its crisis value. In this case a new type of scaling phenomenon is found and discussed. [The example of an interior crisis used in section 2, the sudden widening of three chaotic bands to form one broader band, was first extensively discussed by Chang and Wright [4] (see also Grebogi et al. [3]).]

In section 3 we give two examples from the Hénon map. In the first, previously noted by Simo' [5], a range of the parameter occurs in which two strange attractors, each with its own basin of attraction, coexist. As the parameter is raised, one of the attractors experiences a boundary crisis and is destroyed. Past this point a chaotic transient occurs, and we investigate its characteristics, including the average lifetime of the transient. In addition, the connection between crises and the formation of horseshoes for this example is discussed and illustrated. As a byproduct of our study of this example, we have carried out an extensive numerical examination of the dependence of Lyapunov numbers on initial conditions. To our knowledge, this represents the most systematic and rigorous numerical test and confirmation yet done of the proposition that the same Lyapunov numbers result from almost all initial conditions in some basin of attraction. In our second example utilizing the Hénon map, we consider the effect of having the Jacobian nearly zero (so that the map is nearly one-dimensional) on the intermittent chaos associated with the tangent bifurcations which occur for many parameter values within the chaotic range of the one-dimensional quadratic map. We find that, for small positive Jacobian, the intermittency and tangent bifurcation phenomenon is replaced by a sequence of events involving the coexistence of two attractors and a boundary crisis.

In section 4 we consider examples involving differential equations in three dimensions. We show that, for several examples appearing in the literature, boundary crises are probably present. In particular, the Lorenz attractor provides a clear case [6], in which the onset of chaos takes the form of a sequence of events involving the coexistence of two attractors and a boundary crisis.

In section 5 we describe a special kind of boundary crisis and present an illustrative example. For the example considered the chaotic attractor takes the form of a "fractal" (nowhere differentiable) torus lying in three-dimensional space. There is another fractal torus which forms the boundary of the basin of attraction for the chaotic attractor. As a parameter of the system is raised a boundary crisis occurs in which unstable fixed points on the two tori collide. Above this value of the parameter almost all initial conditions asymptote to infinity.

We wish to emphasize that, although the discussion of boundary crises has so far concerned with the destruction of strange attractors, the inverse process is also necessarily implied. That is, if a parameter is varied from a to b and the strange attractor is destroyed, then when the parameter is varied in the opposite direction, from b to a, the attractor is born. Thus the *sudden* appearance of a strange attractor and its basin is a possible "route to chaos". This sudden appearance is to be contrasted with the routes discussed by Eckmann [7] and called by him "scenarios". In a scenario a non-chaotic attractor changes its character so that it becomes chaotic. In contrast, in the inverse crisis route to chaos, a chaotic transient is converted into a chaotic attractor. For example, the route to chaos, (discussed by Kaplan and Yorke [6]) for the Lorenz attractor is of this type. Also, our discussion in section 5 can be viewed as illustrating a new route to chaos in which chaos appears due to a type of bifurcation which can only occur in invertible maps (flows) of at least three (four) dimensions.

To conclude this section, we note that the Hénon map crisis in section 3 occurs at a parameter value where there is a tangency of the stable and unstable manifolds as illustrated in fig. 13. However, the crisis described in section 5 is different in that no tangency of stable and unstable manifolds occurs (as shown in fig. 29). Thus, the concept of crises (collisions of attractors with unstable fixed points or unstable periodic orbits) cannot be replaced by the older concept of tangencies of stable and unstable manifolds.

2. The one-dimensional quadratic map

The one-dimensional quadratic map,

$$x_{n+1} = C - x_n^2 \equiv F(x_n, C), \tag{1}$$

exhibits the following well-known behavior. For $C < -\frac{1}{4}$ no fixed point of the map exists, and all orbits asymptote to $x = -\infty$. At $C = -\frac{1}{4}$ a tangent bifurcation occurs at which a stable and unstable fixed point are created. For $C > -\frac{1}{4}$ these points are $x = -x_* \equiv -\frac{1}{2} - [\frac{1}{4} + C]^{1/2}$ (unstable) and $x = -\frac{1}{2} + [\frac{1}{4} + C]^{1/2}$ (stable). As C increases

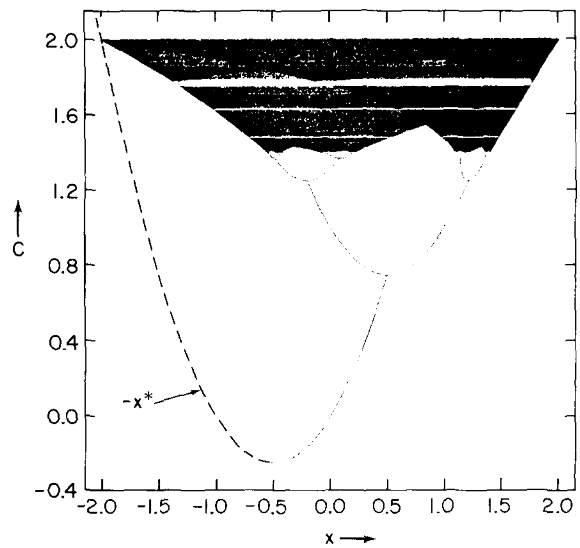

Fig. 1. Bifurcation diagram for the map, eq. (1). The dashed curve is the unstable fixed point. For a given value of C, an initial condition x is chosen and its orbit is plotted after the first several thousand iterates. The first several thousand iterates are discarded in order to ensure that the transient has died away. The figure is generated by doing this for many different values of C.

past $-\frac{1}{4}$, the stable fixed point undergoes period doubling followed by chaos [2]. The basin of attraction for these orbits for $-\frac{1}{4} \leqslant C \leqslant 2$ is $|x| \leqslant x_*$. Thus the unstable orbit, $x = -x_*$, is on the boundary of the basin of attraction. As C is incrased past $C = 2$, the chaotic attracting orbit is destroyed, and almost all initial conditions lead to orbits which approach $x = -\infty$. Fig. 1 gives a bifurcation diagram corresponding to this situation. In this figure the unstable fixed point is plotted as a dashed curve. Note that the destruction of the chaotic attractor and its basin as C increases through $C = 2$ coincides with the intersection of the chaotic band with the unstable fixed point. For C slightly larger than two, a point initialized in the formerly chaotic region will generate a chaotic looking orbit (a chaotic transient) until "by chance" x_n falls into a loss region [cf. discussion following eq. (3)]. After this happens, the orbit rapidly accelerates to large negative values of x. It has been shown [8, 9] that, for a smooth distribution of initial conditions in the formerly chaotic region of x, the length of a chaotic transient, τ, is exponentially distributed [10],

$$\phi(\tau) = \langle\tau\rangle^{-1} \exp-(\tau/\langle\tau\rangle). \tag{2}$$

Letting $\langle\tau\rangle$ denote the expected value of the transient time, eq. (2) means that the probability of observing a transient time in an interval between τ and $\tau + d\tau$ is $\phi(\tau)\, d\tau$ (when an initial condition is chosen at random). Numerical evidence for (2) in higher-dimensional cases will be given in section 3. Furthermore, for $1 \gg C - 2 > 0$, the average length of a chaotic transient, $\langle\tau\rangle$, scales as [9]

$$\langle\tau\rangle \sim (C-2)^{-1/2}. \tag{3}$$

That this should be so can be se seen as follows. For $C - 2 > 0$ there is a region $|x| < (C - x_*)^{1/2} \approx [\frac{2}{3}(C-2)]^{1/2}$, which, on one iterate, maps to $x > x_*$. On one more iterate x is mapped to $x < -x_*$, after which it accelerates to $-\infty$. Thus points which fall in this region are lost. Since the length of the loss region is approximately proportional to $(C-2)^{1/2}$, we expect $\langle\tau\rangle \sim (C-2)^{-1/2}$. It will be demonstrated numerically in section 3 that (3) holds for a two-dimensional case occurring in the Hénon map. The type of crisis illustrated in fig. 1 (namely, one in which the unstable orbit which collides with the chaotic attractor is on the boundary of the basin) we call a *boundary crisis*.

A second type of crisis in which the collision with an unstable orbit occurs within the basin of attraction, herein called an *interior crisis*, is illustrated by the bifurcation diagram shown in fig. 2. Fig. 2 is a magnification of the region in fig. 1 encompassing the tangent bifurcation at which a stable period three orbit is born within the chaotic regime. Also shown in fig. 2 are dashed curves denoting the *unstable* period-three orbit created at the tangent bifurcation. Note from fig. 2 that for a range of C less than a certain critical value, C_{*3}, the chaotic attractor lies within three distinct bands, but that, when C increases past $C_{*3} \approx 1.79$, the three chaotic bands suddenly widen to form a single band. Furthermore, this coincides precisely with the intersection of the unstable period-three

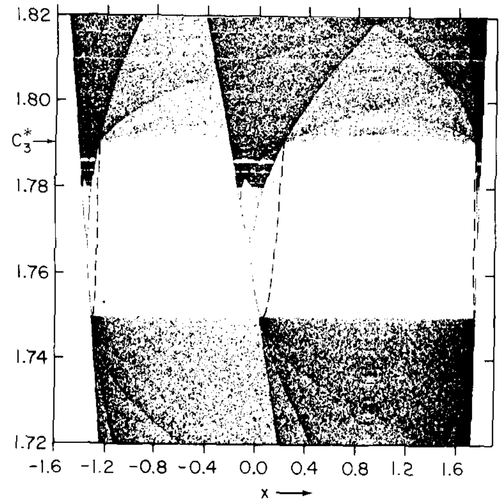

Fig. 2. Blow up of the bifurcation diagram of fig. 1 in the region of the period three tangent bifurcation. The dashed curves denote the unstable period-three orbit created at the tangent bifurcation.

orbit created at the original tangent bifurcation with the chaotic region. Similar crisis-induced widenings are associated with the other tangent bifurcations occurring in the chaotic range (i.e., $C_\infty < C \leqslant 2$, where C_∞ is the accumulation point for period doubling bifurcations of the original stable fixed point). As another example of this, fig. 3 shows a bifurcation diagram for the period five window.

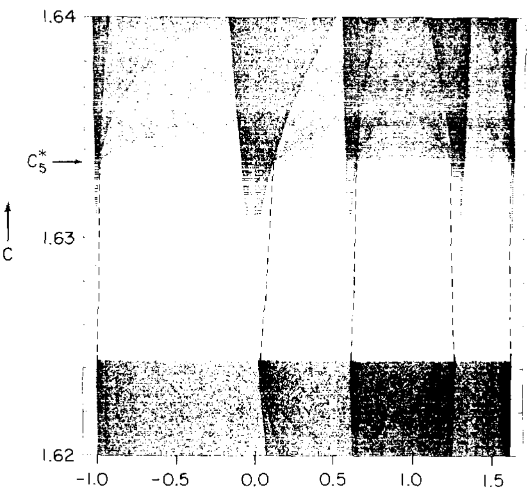

Fig. 3. Bifurcation diagram for the region of the period five tangent bifurcation.

In addition, we also note that figs. 2 and 3 provide examples illustrating that boundary crises are not the only means by which a chaotic attractor may suddenly terminate. Namely, a process that might be called *subduction* can occur. In a subduction a nonchaotic attractor appears within a chaotic attractor, and the chaotic attractor is replaced by the nonchaotic attractor. The effect of a subduction differs from that of a boundary crisis in that a subduction does not destroy the basin of the chaotic attractor, but rather the basin remains unchanged as the chaotic attractor converts to a nonchaotic attractor. Subductions are well-known phenomena in the case of the one-dimensional quadratic map, and correspond to the tangent bifurcations in which non-chaotic periodic orbits appear within the chaotic range. The points $C \approx 1.7499$ and $C \approx 1.6244$ at which the period-three and five orbits are born correspond to subductions (cf. figs. 2 and 3). Examples of subductions occurring in a two-dimensional map will be given in subsection 3.3.

Returning now to our discussion of the interior crisis at $C = C_{*3}$, consider fig. 4a which shows the

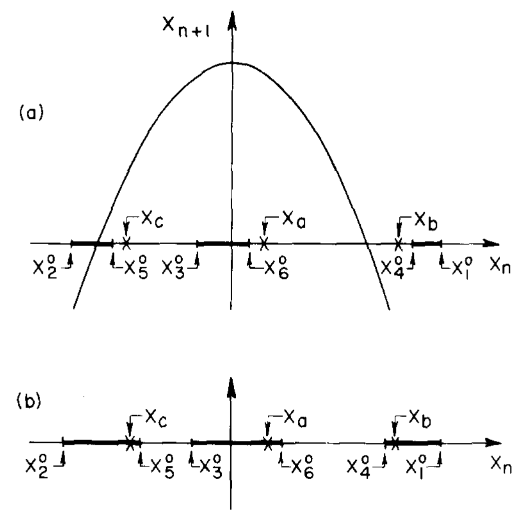

Fig. 4. (a) Schematic illustration of the quadratic map, eq. (1), for a value of C slightly less than C_{*3}. The three chaotic bands are indicated on the x_n-axis with boundary points x_1^0, x_2^0, x_3^0, x_4^0, x_5^0, x_6^0. Also shown as crosses are the components of the unstable period three orbit, x_a, x_b, x_c. (b) Schematic illustration of the x_n-axis for C slightly larger than C_{*3}.

map (1) for a value of C slightly less than C_{*3}. The three chaotic bands are indicated schematically on the x_n axis as the intervals $[x_3^0, x_6^0]$, $[x_4^0, , x_1^0]$, and $[x_2^0, x_5^0]$. Also, the unstable period three points, x_a, x_b, x_c, are indicated as crosses. The rightmost boundary of the chaotic region, x_1^0, is clearly the image of $x = 0$, since $F(x, C)$ is maximum at $x = 0$. Thus, $x_1^0 = F(0, C)$. We denote F composed with itself n times by $F^{(n)}(x, C)$; i.e., $F^{(n)}(x, C) = F[F^{(n-1)}(x, C), C]$, and $F^{(1)}(x, C) \equiv F(x, C)$. Examination of fig. 4 then shows that $x_n^0 = F^{(n)}(0, C)$. Now consider x_4^0. At $C = C_{*3}$, $x_4^0 = x_b$, and hence $x_4^0 = x_7^0$, or $F^{(4)}(0, C_{*3}) = F^{(7)}(0, C_{*3})$. This relation provides a means for the accurate numerical determination of C_{*3}. We obtain $C_{*3} = 1.790327492\ldots$

For C slightly larger than C_{*3}, the unstable orbit x_a, x_b, x_c will lie within the bands, $[x_3^0, x_6^0]$, $[x_4^0, x_1^0]$, $[x_2^0, x_5^0]$, [cf. fig. 4b]; x_a will be slightly less than x_6^0, x_b will be slightly greater than x_4^0, and x_c will be slightly less than x_5^0. An orbit started within one of the regions, $[x_3^0, x_a]$, $[x_b, x_1^0]$, $[x_2^0, x_c]$, will typically *initially* move about in a chaotic way, cycling among the three regions, as in the case $C < C_{*3}$. However (for C slightly larger than C_{*3}), the orbit will eventually fall within one of the small regions $[x_a, x_6^0]$, $[x_4^0, x_b]$, $[x_c, x_5^0]$. It will then be repelled by the unstable period-three orbit and be pushed into the formerly empty region, namely $[x_6^0, x_4^0]$ and $[x_5^0, x_3^0]$. The discussion of fig. 4 just given parallels the treatments in refs. 3 and 4 (cf. also ref. 11).

Figs. 1 and 2 illustrate three examples of general types of sudden changes of chaotic orbits: the tangent bifurcation (in which a chaotic orbit is converted to a periodic one; this is not a crisis but a subduction), the boundary crisis (in which the chaotic attractor and its basin are destroyed), and the interior crisis (in which a sudden widening of the chaotic attractor occurs). What is the characteristic behavior of an orbit when the parameter is near a point at which a sudden change in chaotic dynamics occurs? For a tangent bifurcation the answer is intermittency [12]. For a boundary crisis the answer is a chaotic transient [8–10]. To answer the question for the case of an interior crisis, consider the fraction of time which an orbit spends in the formerly empty region, $[x_5^0, x_3^0]$ and $[x_6^0, x_4^0]$. We let $c \equiv C - C_{*3}$ and denote the fraction by $f(c)$. We now attempt to predict the form of $f(c)$ for $c \ll 1$. The trajectory generally spends a long time (denote the average τ_2) in the old regions (namely $[x_3^0, x_6^0]$, $[x_4^0, x_1^0]$ and $[x_2^0, x_5^0]$) before being pushed into the new region. There it spends an average time τ_1 before returning to the old region, and the process continues back and forth. Since we are concerned with an invariant distribution, we balance the transfer rates between the two regions, $f/\tau_1 = (1-f)/\tau_2$. Since $c \ll 1$, we have $f \ll 1$, and thus $f(c) \approx \tau_1/\tau_2$. To estimate τ_2, we follow the argument leading to eq. (3) and consider the interval $[x_3^0, x_a]$. For $c > 0$ an interval about $x = 0$ will be mapped by $F^{(3)}$ to $[x_a, x_6^0]$ and then be repelled into the formerly empty region. Since F and hence $F^{(3)}$ have quadratic extrema about $x = 0$, the length of this loss region centered at $x = 0$ is proportional to $c^{1/2}$. Hence we estimate that $\tau_2 \sim c^{-1/2}$. To estimate τ_1, consider the action of the map on the interval $[x_a, x_b]$. Since $x_a \to x_b$ and $x_b \to x_c$, the interval is inverted and stretched between x_c and x_b. Thus some range near the middle of the formerly empty region $[x_6^0, x_4^0]$ is mapped into $[x_3^0, x_a]$. We denote this range near the middle of $[x_6^0, x_4^0]$ by $[x_\alpha, x_\beta]$. The lifetime of an orbit in the formerly empty region is essentially determined by the time it takes to land in $[x_\alpha, x_\beta]$ after which it gets kicked back into the old region. Let λ denote the linear stability parameter of the unstable period-three orbit, $\lambda = F^{(3)\prime}(x_a) = F'(x_a)F'(x_b)F'(x_c)$, where $F'(x) \equiv \mathrm{d}F(x)/\mathrm{d}x$. At $c = 0$, $\lambda = 3.714\ldots$. Consider iterates of the point $x = 0$ under the application of $F^{(3)}$. For $1 \gg c > 0$, on two applications of $F^{(3)}$ the image of $x = 0$ falls just to the right of x_a [cf. fig. 4b]. Since, for small c, this image x_6^0, is close to x_a, $(x_6^0 - x_a \sim c)$ the linear approximation is valid. On n further applications of $F^{(3)}$, the distance from x_a increases as λ^n. Thus the time it takes the orbit to exceed x_α is approximately $(\ln c^{-1})/(\ln \lambda)$, that is $x_\alpha - x_a \sim c\lambda^n$. Say that, for a particular value of c, after $\bar{\tau}$ iterates, x_6^0 falls exactly on x_α. As c is increased further the orbit will fall into $[x_\alpha, x_\beta]$ and be lost. On further increase of c the $\bar{\tau}$ iterate of x_6^0 will exceed x_β with the $\bar{\tau} - 1$ iterate of x_6^0 still less than x_α. When this happens τ_1 increases above $\bar{\tau}$. On still further increase of c, the $\bar{\tau} - 1$ iterate of x_6^0 will fall on x_α, and the whole process will repeat. Based on the above picture of the process whereby orbits get fed back into the region of high density, we estimate that $\tau_1 \approx \tau_\alpha + P(\ln c)$, where $\tau_\alpha = \eta^{-1} \ln c^{-1}$, $\eta = \ln \lambda$, and P is a periodic function of period η. Hence, from $f(c) \approx \tau_1/\tau_2$, we have

$$f(c) \approx K[c^{1/2}P(\ln c^{-1}) + \eta^{-1}c^{1/2}\ln c^{-1}]. \tag{4}$$

Note that the first term in eq. (4), $f_1(c) \equiv Kc^{1/2}P(\ln c^{-1})$, possesses scale invariance, $f_1(\lambda c) = \lambda^{1/2} f_1(c)$. That is, if we look at a graph of $f_1(c)$ and then properly magnify it about the origin, it will look the same. Fig. 5 shows a graph of $f(c)/c^{1/2}$ versus $\ln c$ which has been numerically generated by iterating the map. The result support eq. (4) including the predicted period $\eta \approx 1.312$. [It may be that a renormalization group analysis of this scaling behavior could succeed in obtaining the function P of eq. (4).]

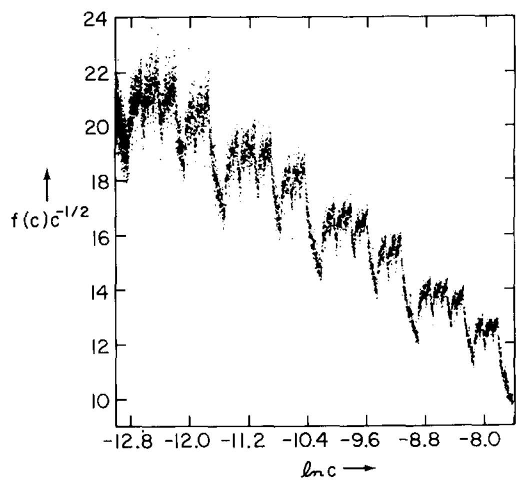

Fig. 5. $f(c)/c^{1/2}$ versus $\ln c$. $c = C - C_{*3}$.

3. The Hénon map

In this section we shall discuss two examples of crisis within the context of the well-known quadratic, two-dimensional, invertible map introduced by Hénon,

$$x_{n+1} = 1 - \alpha x_n^2 + y_n, \tag{5a}$$

$$y_{n+1} = -Jx_n. \tag{5b}$$

Note that the parameter J is the determinant of the Jacobian matrix of the map and that, for $J = 0$, eq. (5a) reduces to the one-dimensional quadratic map, $x_{n+1} = 1 - \alpha\, x_n^2$ (which can be transformed into (1) by the change of variables $\alpha x \to x$).

In subsection 3.1 we discuss a boundary crisis occuring for (5) for a case with large Jacobian determinant ($J = -0.3$). In subsection 3.2 we investigate the connection between crises and horseshoe formation. Then, following that, subsection 3.3 discuss how certain results from the one-dimensional map ($J = 0$) are modified by a small amount of two dimensionality (i.e., small J), and the role of crises in this phenomenon is pointed out.

3.1. *An example of a boundary crisis*

We consider the Hénon map for $J = -0.3$. It has been pointed out [5] that, for this J and a range of α, two attractors can exist simultaneously. Numerical results for $\alpha = 1.0807000$ are shown in figs. 6–10. For this value of α the two coexisting attractors are both chaotic. One attractor consists of four pieces on which an orbit on the attractor cycles sequentially. The other attractor consists of six pieces on which its orbit similarly cycles. Fig. 6 shows the basins of attraction for the six-piece chaotic attractor in black and that for the four piece chaotic attractor in white. Also shown in fig. 6 is the four-piece attractor. Fig. 7 shows both the four-piece attractor (A1, ..., A4) and the six-piece attractor (B1, ..., B6). Note that an unstable (saddle) fixed point of the map is located at $x = 0.69113...$, $y = 0.20734...$ (labeled FP in fig. 7). The stable and unstable manifolds of this fixed point are shown in fig. 8. Comparison of figs. 7 and 8 suggests that the two attractors lie on the closure of the unstable manifold of the fixed point. From fig. 6 fine scale structure in the basins of attraction

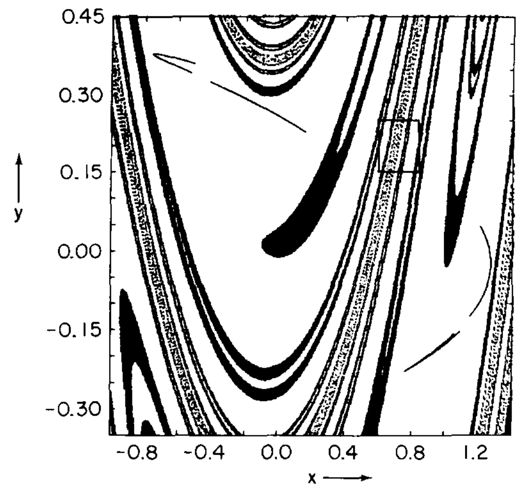

Fig. 6. Basins of attraction for the six-piece chaotic attractor (black) and the four-piece chaotic attractor (blank) for $\alpha = 1.0807000$ and $J = -0.3$. Also shown is the four-piece chaotic attractor.

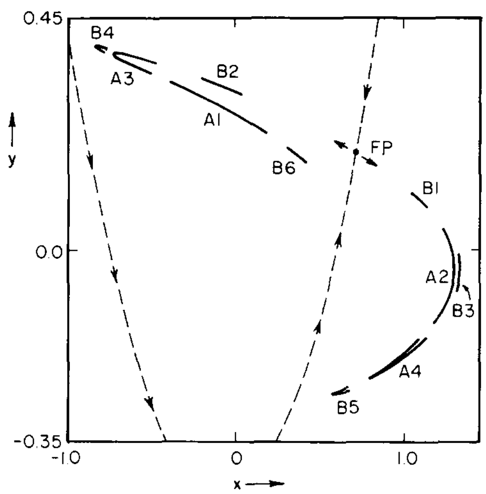

Fig. 7. Orbits on the four-piece attractor cycle from segment A1 to A2 to A3 to A4 and back to A1. Orbits on the six-piece attractor also cycle (B1→B2→···→B6→B1). The parameter value is the same as in fig. 6. The stable manifold of the unstable saddle fixed point FP is shown (as a dashed line) and the unstable directions are indicated.

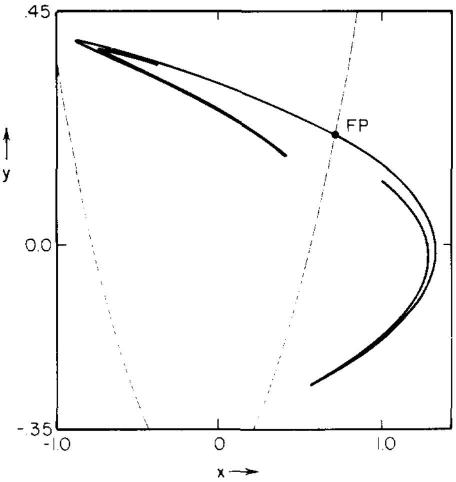

Fig. 8. The stable manifold (dashed line) and unstable manifold (continuous line) of the fixed point FP for the same parameter value as in figs. 6 and 7.

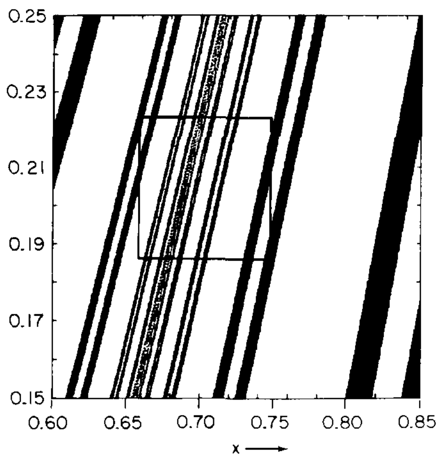

Fig. 9. Blow up of the boxed region in fig. 6.

is apparent. To see this more clearly, fig. 9 presents a blow up of the boxed region in fig. 6. This box was chosen so that the fixed point of the map at $x = 0.69113 \ldots$, $y = 0.20734\ldots$ is at the box's center. The eigenvalues of the Jacobian matrix of the map at the saddle fixed point are $\bar{\lambda}_u = -1.6731\ldots$ and $\bar{\lambda}_s = 0.17931\ldots$. The eigenvector associated with $\bar{\lambda}_u$ is of course tangent to the unstable ($|\bar{\lambda}_u| > 1$) manifold of the fixed point, while the eigenvector associated sigh $\bar{\lambda}_s$ is tangent to the stable manifold of the fixed point. The stable manifold (also shown as a dashed line in fig. 7) is in the direction along the bands of fig. 9, while the unstable manifold cuts across them. Now consider what happens if we apply the inverse map to fig. 9. Bands crossing the unstable manifold will be drawn in towards the fixed point, shrunk in width (by approximately $|\bar{\lambda}_u|^{-1}$), flipped to the other side of the fixed point (because $\bar{\lambda}_u$ is negative), and stretched out along the stable manifold (by $1/\bar{\lambda}_s$). (Thus the fine scale structure seen in fig. 6 aligns along the stable manifold of the fixed point.) To further demonstrate the above, we magnify the region about the fixed point in fig. 9 by a factor $\bar{\lambda}_u^2$. The result, fig. 10, reproduces fig. 9, thus showing clearly the scaling of the basins of attraction about the fixed point.

We now discuss how the basin of attraction diagrams, figs. 6, 9 and 10, were constructed. Numerically it is found that the positive Lyapunov exponents for the map are $h_4 = 0.1391\ldots$ (corresponding to the four-piece attractor) and $h_6 = 0.1097\ldots$ (corresponding to the six-piece attractor). We choose an x–y grid of 1.09×10^4 initial conditions. We then iterate the map and its Jacobian and calculate the resulting Lyapunov exponent. For every initial condition tested we find that the computed Lyapunov number falls within either the interval $[h_4 - 5 \times 10^{-4}, h_4 + 5 \times 10^{-4}]$ or

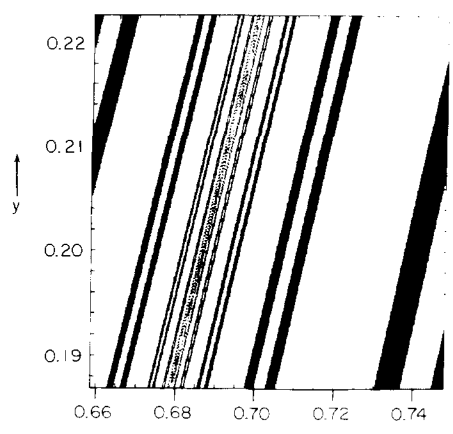

Fig. 10. Blow up of the boxed region in fig. 9.

the interval $[h_6 - 5 \times 10^{-4},\ h_6 + 5 \times 10^{-4}]$. (Presumably the tolerances would be reduced if the number of iterates of the map was increased.) When a Lyapunov exponent falls within the latter interval, we plot its initial condition as a dot. Because of the high density of initial conditions, the six-piece attractor basin is completely filled in as the black regions of figs. 6, 9 and 10. In no case does an isolated black dot occur in a white region and vice versa.

The above described result indicates that, from a practical numerical point of view, the Lyapunov numbers are essentially independent of the choice of initial point in the basin (i.e., we saw only two ranges rather than a much larger class of Lyapunov numbers). While this appears to be a reasonable a priori assumption and is basic to a number of previous studies, its validity does not appear to have been previously tested as intensively as was done here.

Returning now to the issue of how the dynamics change as a parameter is varied, fig. 11 shows a bifurcation diagram (α versus x) for a range of x which encompasses one segment each of the four piece and the six-piece attractors. The six-piece attractor is created at $\alpha = \alpha_0 \equiv 1.062371838\ldots$ by a saddle-node bifurcation in which an attracting period-six orbit and an unstable saddle type period-six orbit simultaneously appear. The position of the saddle is shown as a dashed line in the figure. The stable manifold emanating from the saddle forms the boundary separating the basins of attraction for the two attractors. As α is increased past α_0, the stable period-six orbit undergoes period doubling followed by chaos. Finally at $\alpha = \alpha_c = 1.080744879\ldots$ a crisis occurs, and the six-piece attractor ceases to exist for $\alpha > \alpha_c$. The evolution of a segment of the six-piece attractor (B5 of fig. 7) and the basin boundary, as α approaches α_c from below, is illustrated in fig. 12. The location of the unstable period-six saddle (which was created at $\alpha = \alpha_0$) is indicated in fig. 12. The collision of the chaotic attractor and the saddle on the basin boundary is evident. From fig. 12c we see that at the crisis, $\alpha = \alpha_c$, a "finger"-shaped region of the four-piece attractor basin comes down and touches the six-piece attractor. This results from a backwards iterate of the region around the apparent tangency point of the attractor and the basin boundary at the left of the figure. Furthermore, there are, in fact, an infinite number of such fingers, accumulating at the unstable saddle. These fingers correspond to higher order backwards iterates of the tangency region at the left of the figure, but are so narrow that they are not visible in fig. 12c.

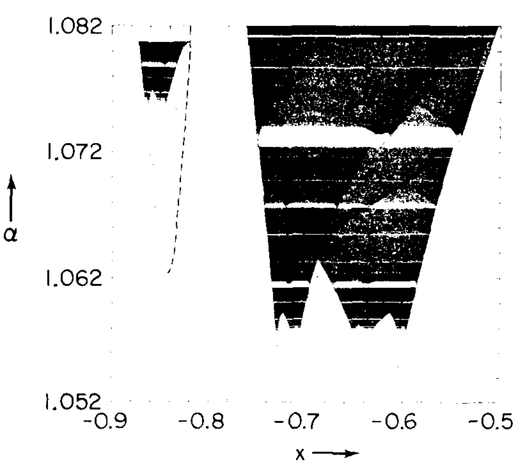

Fig. 11. Bifurcation diagram for eq. (5) with $J = -0.3$.

Generally, for the examples discussed in this paper, we find that, when a crisis approaches, it seems that the attractor lies in the closure of the unstable manifold of the periodic orbit that it is about to collide with. Thus the evolution of the attractor shown in fig. 12 may also be discussed in terms of stable and unstable manifolds of the saddle [5]. The six-piece attractor apparently lies on the unstable manifold of the saddle (compare figs. 7 and 8). Thus, as the crisis is approached, the stable manifold (basin boundary) and the unstable manifold approach each other, becomes tangent ($\alpha = \alpha_c$), and then cross ($\alpha > \alpha_c$). The situation for $\alpha = \alpha_c$ is schematically illustrated in fig. 13. Near the crisis ($\alpha = \alpha_c$), the results of Newhouse [13] imply that there can be an infinite number of attractors. Our numerical results, however, have only succeeded in finding the original six- and four-piece attractors. Thus any other attractors must be difficult to detect (e.g., their basins may be very small).

Fig. 14 shows successive iterates of an orbit initialized in the former basin of attraction of the six-piece attractor for α slightly larger than α_c ($\alpha = 1.0807455$). The numbers indicate the sequence in which points appear in the figure. Thus after the first iterate the orbit rapidly approaches the remnant of the destroyed attractor. The orbit then bounces around on this remnant roughly 2,000 times, until it finds its way out, and then rapidly goes to the four-piece attractor. Fig. 15

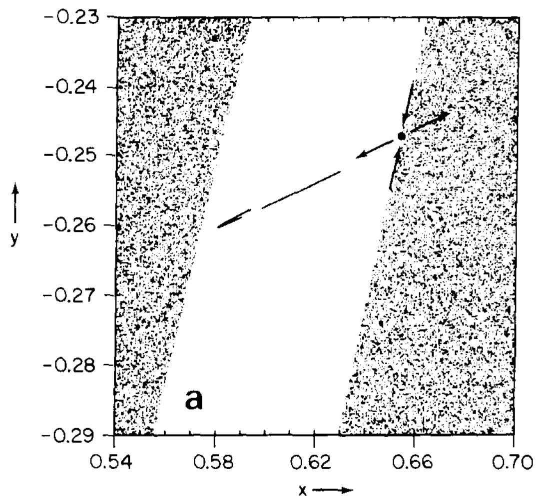

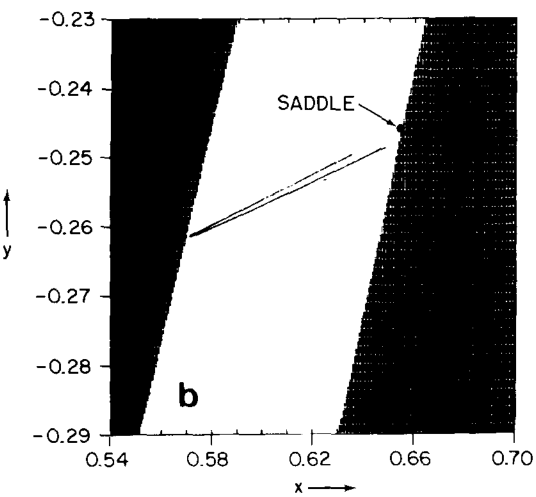

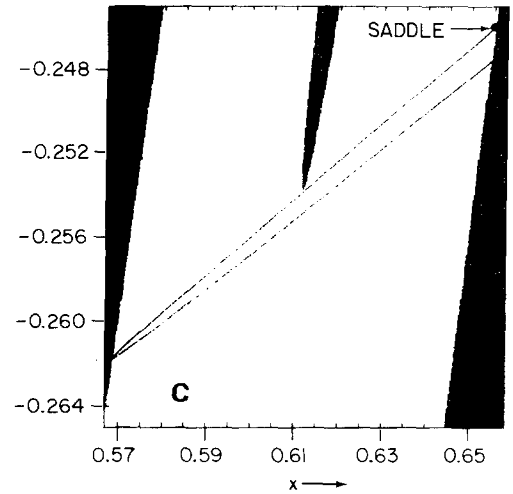

Fig. 12. (a) A segment of the six-piece attractor in its basin for $\alpha = 1.0770000$, $J = -0.3$. The location of one component of the period-six saddle and its stable and unstable directions are indicated. The region filled in with dots denotes the basin of the four-piece attractor. (For this value of α each segment of the "six-piece" attractor consists of two pieces so it is really a twelve-piece attractor). (b) $\alpha = 1.0800000$. (c) $\alpha = 1.0807430$.

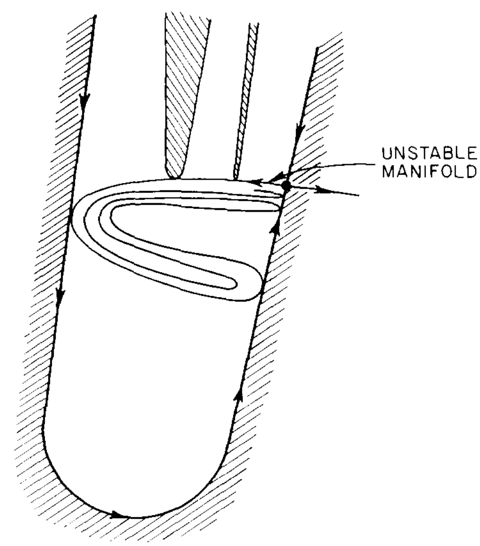

Fig. 13. Schematic diagram of the stable and unstable manifolds of the saddle for $\alpha = \alpha_c$. The stable and unstable manifolds of the saddle become tangent at an infinite number of points.

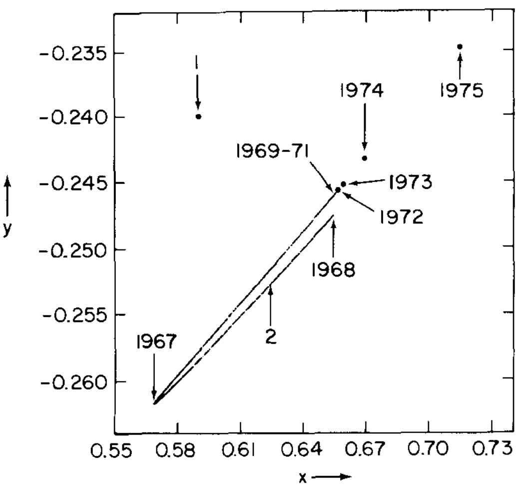

Fig. 14. Iterates of the map for $\alpha = 1.0807455 > \alpha_c$.

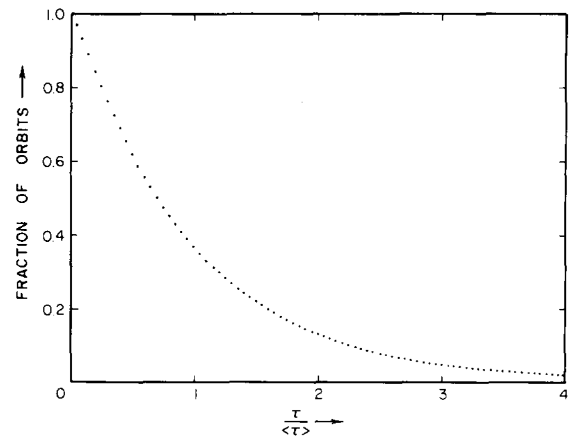

Fig. 16. Numerical results for fraction of orbits remaining on the remnant of the chaotic attractor as a function of time. These results were obtained for eq. (5) for $J = -0.3$ and $\alpha = 1.08007500$, using data from 10^5 initial conditions randomly chosen within the rectangular region $x \in (0.59000, 0.59125)$ and $y \in (-0.64000, -0.63875)$. $\langle \tau \rangle = 1753.6$.

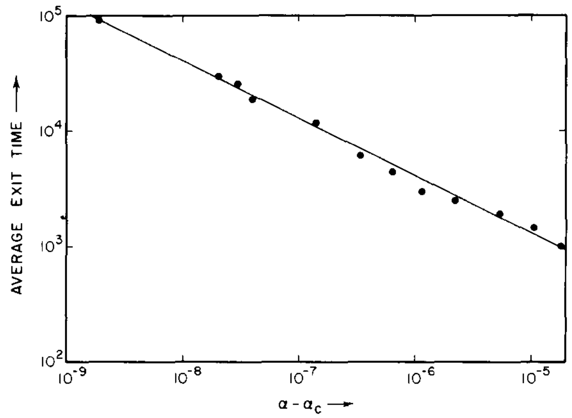

Fig. 15. Average lifetime of a chaotic transient obtained by numerical iteration of eq. (5) with $J = -0.3$ (dots) and theoretical predicted proportionality to $(\alpha - \alpha_c)^{-1/2}$ eq. (3) (straight line). Each point was obtained by averaging 10^2 initial conditions randomly chosen into the rectangular region $x \in (0.59000, 0.59125)$ and $y \in (-0.64000, -0.63875)$.

shows results from a numerical test (dots) of eq. (3) (straight line) (see captions for details). As can be seen from the figure the agreement is quite good. Fig. 16 shows numerical results (dots) testing eq. (2). On the scale of this figure there is no discernible difference between the numerical data and the exponential decay predicting of eq. (2).

3.2. *Protohorseshoes become horseshoes via crises in the Hénon map*

In this subsection we discuss the formation of a horseshoe associated with the six-piece attractor. The formation of horseshoes is sometimes thought to be associated with the appearance of chaotic attractors. In contrast, for our example we find that the horseshoe which we consider forms at some value of α greater than α_c. That is, it forms after the chaotic attractor has already been destroyed. In fact, as subsequent discussion will show, the destruction of the attractor appears to be a natural consequence of the formation of the horseshoe. On the other hand, we also find that before the horseshoe forms another configuration, which we call a *protohorseshoe*, exists, and that the attractor is contained within the protohorseshoe. Further, some of the observed aspects of the evolution of the six-piece attractor as α increases can be understood by considering the evolution of the protohorseshoe as it changes into a horseshoe.

A horseshoe [14] is a rectangle (or topological rectangle) whose image forms a horseshoe-like shape as shown in fig. 17(i). In this figure the rectangle has sides ABCD and its image sides A′B′C′D′. We have numerically taken the image of a rectangle in the region shown in fig. 12. The result is shown in fig. 17(iv), for $\alpha = 1.085 > \alpha_c$. It is seen that a horseshoe exists. Subject to certain regularity hypotheses it may be shown that there are infinitely many unstable periodic points in a horseshoe. Horseshoes do not contain attractors. As we vary parameters, the image of the rectangle will change, and we may no longer find a horseshoe. However, herein lies a practical problem: as the parameter is varied the sides of the rectangle can be varied in quite a few ways, and making a non-optimal choice of the sides will sometimes be the reason we no longer find the horseshoe. To aid in the procedure we will describe a way of choosing an optimal placement of sides A and C in fig. 17(i). In this figure, part of the rectangle at side A could be peeled off the rectangle and discarded. Then, the end of the image at A′ would also be shortened. We could imagine whittling down side A, peeling off slices from the rectangle until the new A had an image A′ which would lie on A as shown in fig. 17(ii). We may similarly peel from side C so that the new image C′ lies on A as in fig. 17(iii). We will call this configuration a *reduced* horseshoe. We pay less attention to the placement of B and D. As the parameter of the map is varied, the sides A and C should be moved continuously so that we have a reduced horseshoe for each parameter value. Results proved for horseshoes, about the existence of unstable periodic orbits by Smale [14], are also valid for reduced horseshoes. Notice that in fig. 17(iii), side A is mapped into itself and so generally has a fixed point P. The contraction of A leads to the realization that A lies on the stable manifold of P, and, since C is mapped onto the stable manifold, C is also a segment of the same stable manifold of P (cf. fig. 13). Also, from the action of the map illustrated in fig. 17, generally there will be another fixed point, labeled Q in fig. 17(iii). For the example of subsection 3.1, the points P and Q correspond to those originally created by the saddle-node bifurcation at $\alpha = \alpha_0$.

In fig. 18(i) we show what we call a *proto-*

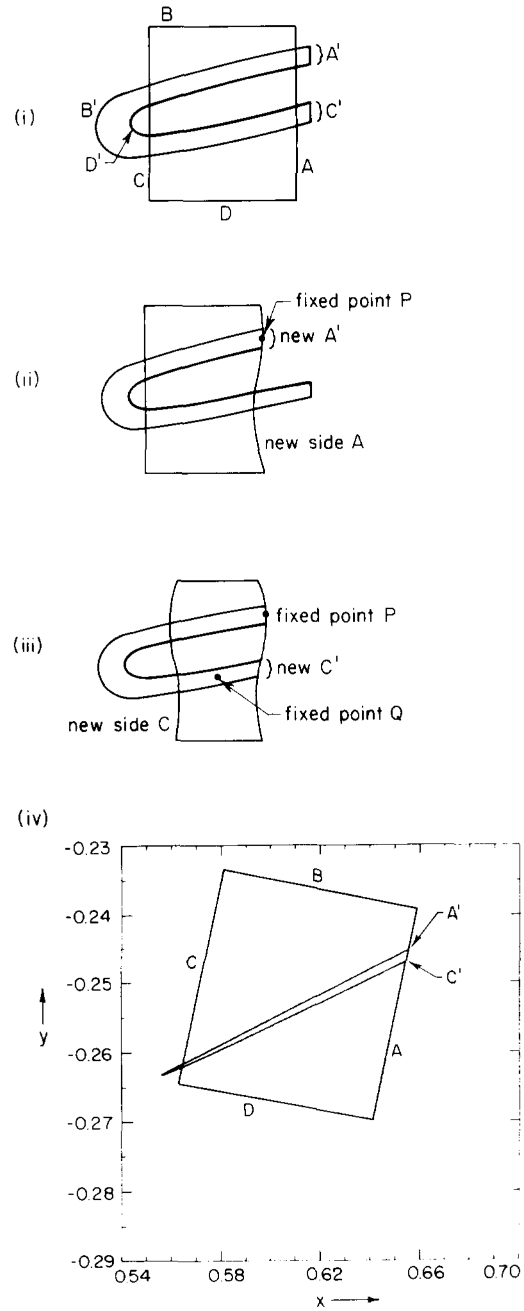

Fig. 17. A horseshoe is a topological rectangle ABCD whose image A′B′C′D′ lies as shown in (i). The lettering of the sides is done for the case when the Jacobian is positive since otherwise B′ and D′ would be reversed. (ii) and (iii) show the steps in constructing a reduced horseshoe. (iv) Horseshoe generated numerically for the piece of attractor shown in fig. 12 ($\alpha = 1.085 > \alpha_c$). The horseshoe appears to be only a line because of the strong contraction along the stable direction.

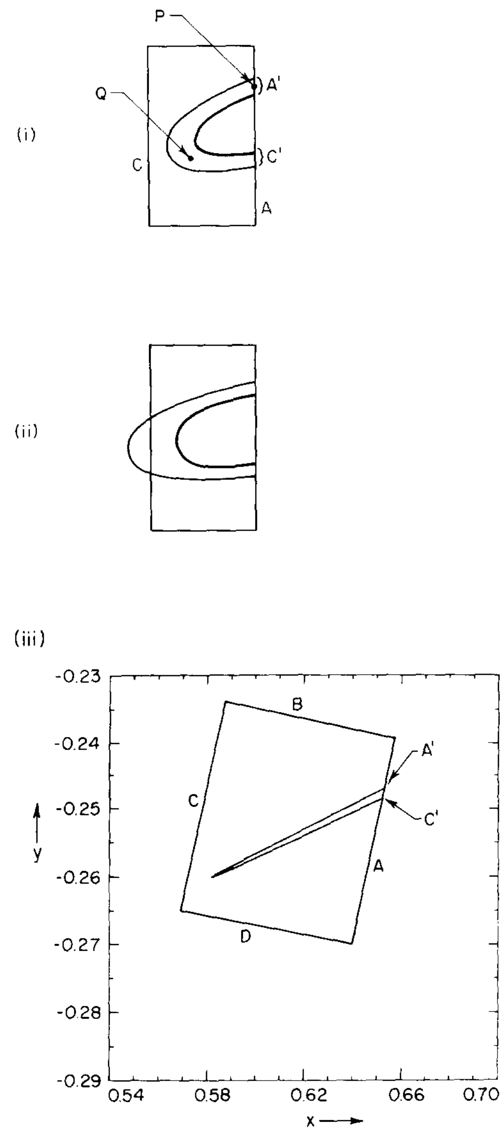

Fig. 18. (i) Protohorseshoe containing two fixed points P and Q with P on side A′ and Q in the interior. (ii) Intermediate stage. (iii) Numerically generated protohorseshoe for the piece of the attractor and the same map parameter ($\alpha = 1.077 < \alpha_c$) as shown in fig. 12.

horseshoe. Since the original ABCD is mapped into itself the protohorseshoe must contain an attractor. Protohorseshoes for the sixth iterate of the Hénon map can be found for $\alpha_0 < \alpha < \alpha_c$ (cf. fig. 18(iii)). The protohorseshoe of the sixth iterate of the Hénon map contains a fixed point [Q in fig. 18(i)] that is attracting for $\alpha_0 < \alpha < 1.0709\ldots$. Thereafter follows a period-doubling sequence and chaos, all of these periodic and chaotic attracting orbits lying in the protohorseshoe. Finally, past $\alpha = \alpha_c$, a boundary crisis occurs, and it is no longer possible to find sides B and D to construct a protohorseshoe. On further increase of α sufficiently past α_c the protohorseshoe of fig. 18(i) evolves into the reduced horseshoe shown in fig. 17(iii) (an intermediate stage in this process is shown in fig. 18(ii)). [However, it should also be noted that, as soon as $\alpha > \alpha_c$, it may be possible to construct a horseshoe (or reduced horseshoe) for some rectangle and some *sufficiently large* iterated image of it. In contrast, the horseshoe and protohorseshoe of figs. 17 and 18 pertain to the rectangle and its first image (or, in the case of the Hénon six-piece attractor, the sixth iterate of the map).]

3.3. *The effect of adding small two-dimensionality to the one-dimensional quadratic map*

We have investigated the effect of small J in eqs. (5). Since $J = 0$ corresponds to the one-dimensional quadratic map, small J may be viewed as a two-dimensional perturbation of the one-dimensional case. Numerically, the most striking effect occurring for small J is the modification of the tangent bifurcation phenomenon (subduction) which for $J = 0$ occurs throughout the chaotic range of α. Fig. 19 shows a bifurcation diagram for $J = 0.015$ and α in a range corresponding to the period-three window in the one-dimensional case (cf. fig. 2). Note that for $1.746\ldots > \alpha > 1.713\ldots$ two attractors are present, the original attractor and one which is born by a period-three saddle-node bifurcation at $\alpha \approx 1.713$. As α is increased to $\alpha \approx 1.746$ a boundary crisis ocurs in which the unstable period three saddle (dashed line in fig. 19) collides with the original chaotic attractor. Fig. 20 shows the basin of attraction for the original chaotic attractor (white region), the original chaotic attractor itself, the basin of attraction of the newly created attractor (black region), and the position on the basin boundary where the period

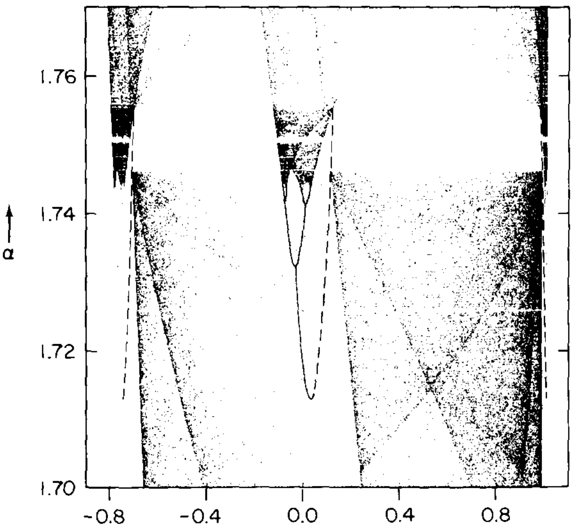

Fig. 19. Bifurcation diagram for $J = 0.015$.

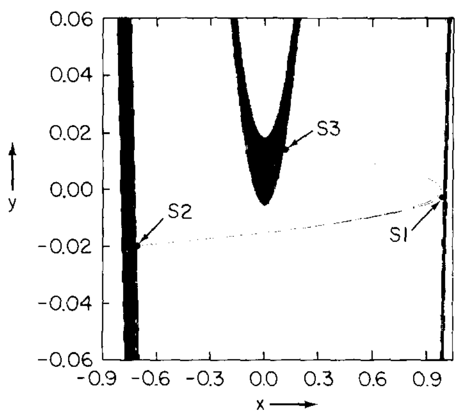

Fig. 20. Original chaotic attractor, period-three unstable saddle $\{S1, S2, S3\}$, and basin of the attractor created at the saddle-node bifurcation (dark region). $\alpha = 1.7300000$, $J = 0.020$.

three saddle $\{S1, S2, S3\}$ is located, for a case in which both attractors exist simultaneously. As α increases further, the period-three saddles collides with the now chaotic three-piece attractor originally created at $\alpha \approx 1.713$. This collision at $\alpha \approx 1.756$ is an interior crisis similar in effect to what happens in the one-dimensional case (i.e., a sudden widening of the three chaotic bands to form one broader chaotic band). The phenomenon illustrated in fig. 19 has been found experimentally [15].

Figs. 19 and 20 correspond to a case with small positive J, and it is evident that, for the case shown, the tangent bifurcation and intermittency phenomenon (or subduction) is replaced by a sequence involving first a saddle-node bifurcation then hysteresis (i.e., two attractors exist simultaneously), then a boundary crisis, and then an interior crisis. Actually, we can show with heuristic arguments that the sequence described is only expected if J exceeds some critical value, J_*, where J_* is small and positive (numerically we find that $J_* < 10^{-3}$ for the period-three window). For $J < J_*$ the original one-dimensional subduction sequence still occurs (see fig. 21 which corresponds to $J = -0.025$).

Also we note that as J increases and passes a second critical value $J'_* > J_*$, the sequence of events illustrated in fig. 19 again alters. Namely, the order in which the unstable saddle orbit hits the two chaotic attractors is interchanged. The result, illustrated in fig. 22 for $J = 0.025$, is first a boundary crisis destroying the now-chaotic three-piece attractor produced by the saddle-node bifurcation

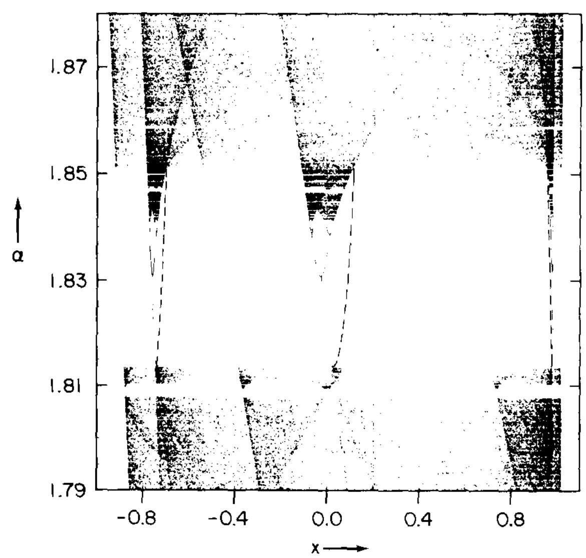

Fig. 21. Bifurcation diagram for $J = -0.025$.

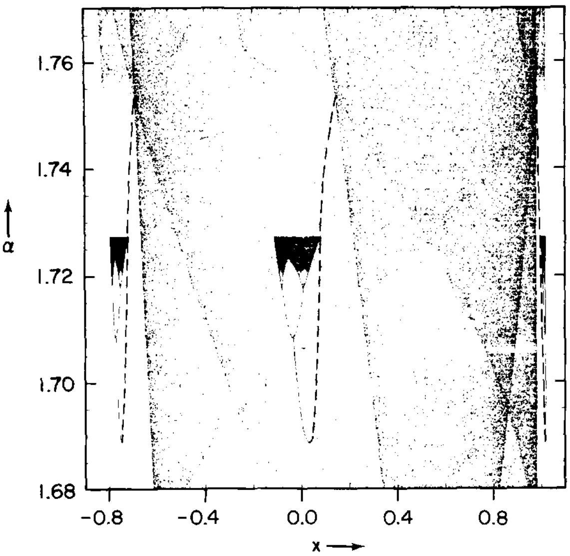

Fig. 22. Bifurcation diagram for $J = 0.025$.

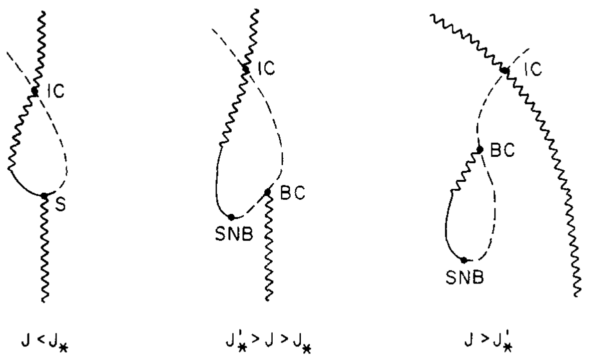

Fig. 23. Crisis diagrams for $J < J_*$, $J'_* > J > J_*$ and $J > J'_*$. IC, BC, SNB and S denote, interior crisis, boundary crisis, saddle node bifurcation and subduction, respectively.

and then an interior crisis giving a sudden widening of the original chaotic single band attractor.

Fig. 23 schematically summarizes the sequences of events occurring for the three cases, $J < J_*$, $J_* < J < J'_*$, and $J > J'_*$. We call the symbolic representations given in fig. 23 "crisis diagrams". In these crisis diagrams the parameter α is taken to increase vertically, a chaotic attracting orbit is represented by a wiggly line, an unstable periodic orbit by a dashed line, and a stable non-chaotic orbit is represented by a solid smooth line. Also fig.

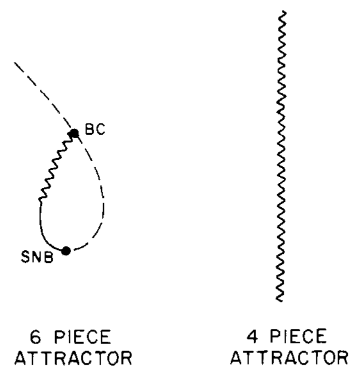

Fig. 24. Crisis diagram for phenomena described in subsection 3.1.

24 gives the crisis diagram for the evolution of the sequence involving the six-piece and four-piece attractors discussed in subsection 3.1 (cf. fig. 11).

In order to explain the results just shown, consider the schematic diagram, fig. 25, corresponding to $J > J_*$ and α slightly larger than its value at which the saddle-node bifurcation occurs (similar to fig. 20). In this figure a strange attractor and an attracting periodic orbit denoted {P1, P2, P3}, where P1→P2→P3→P1, exists simultaneously. Notice that the point P1 lies outside the original attractor's "elbow". This figure illustrates a common geometric inter-relationship that often occurs when two attractors coexist. For example, a situ-

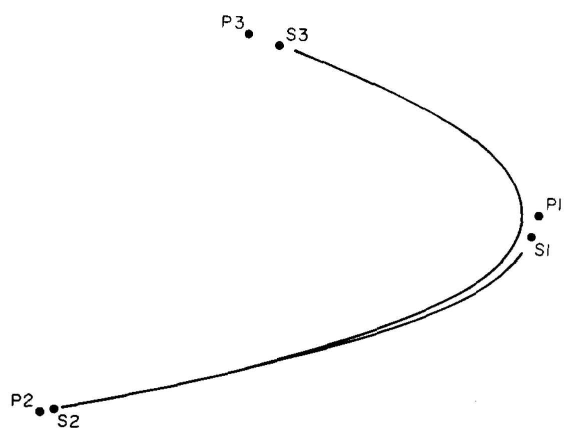

Fig. 25. Schematic representation of coexisting chaotic and periodic {P1, P2, P3} attractors (positive Jacobian). {S1, S2, S3} is the period-three unstable saddle.

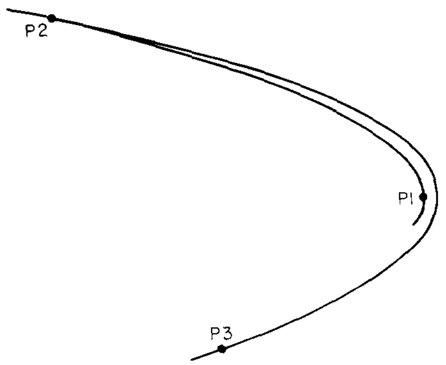

Fig. 26. Schematic diagram of the chaotic attractor at subduction (negative Jacobian).

ation similar to that in fig. 25 is seen in fig. 7, where the attractor piece B3 lies beyond the elbow of attractor A. Had fig. 7 been drawn at $\alpha = 1.065$ instead of 1.0807, the attractor piece B3 would have been a single point outside the elbow. For fig. 7, the periodicity is 6 (even) and the Jacobian of the map of the sixth iterate of the Hénon map is $(-0.3)^6$, a positive number. The simultaneous existence of the two attractors depends crucially on the orbit being beyond the elbow. Figs. 21 and 26 show what happens when the orbit appears inside the elbow. Here J is negative. Fig. 26 is a schematic representation of the chaotic attractor precisely at subduction ($\alpha \approx 1.813$ in fig. 21). The chaotic attractor becomes the periodic attractor {P1, P2, P3} due to a saddle-node bifurcation. In this case, the nature of the elbow of the chaotic attractor near P1 is that it bends tight on iteration. In fig. 7, the elbow piece A2 bends to become A3, and B3 to become B4, the piece B4 lying beyond the end of attractor A. Referring now to fig. 26, if it is assumed that the periodic orbit lies inside the elbow, but off the attractor, the bending elbow entangles the periodic points within the attractor as the map is iterated. Thus there is no separation between the orbit and the attractor, and the orbit must actually lie on the attractor as in fig. 26. The apparently contradictory idea of {P1, P2, P3} being an attractor and being in the chaotic attractor is resolved by noting that the chaotic attractor is actually destroyed by the appearance of the attracting periodic orbit. The distinction between the inside and outside cases lies in the Jacobian. When the Jacobian (or rather the Jacobian raised to the pth power, where p is the period) is negative, it can be argued that the periodic orbit lies inside and its appearance instantly destroys the chaotic attractor (so we have subduction). When the Jacobian is positive, however, it is possible for the saddle-node bifurcation to occur outside the attractor, in which case subduction no longer occurs. (Actually, as previously mentioned, subduction still takes place for J positive but small i.e., $0 < J < J_*$.)

4. Ordinary differential equations

The occurrence of crisis in differential equations is illustrated by at least three examples occurring in the literature: (a) the Lorenz attractor [6, 10, 16], (b) an example occurring in plasma physics [17], and (c) an example involving a study of Josephson junction diodes [18]. Examples (a) and (b) deal with autonomous systems of three first order ordinary differential equations, while example (c) concerns a nonautonomous second order ordinary differential equation. Thus all three cases may be viewed as describing flows in a three-dimensional phase space. For examples (b) and (c), the existence of crises has not been explicitly demonstrated, but we view the evidence as strongly suggestive of crises. For the more well-studied Lorenz attractor, however, the work of Kaplan and Yorke [6] directly implies the existence of a crisis. In all three cases a common pattern occurs. Namely, in some range of a parameter p, say $p_a > p > p_b$, a nonchaotic attractor exists; while in some other range $p_2 > p > p_1$ a chaotic attractor exists. Furthermore for all three cases, $p_a > p_1$. The situation is as illustrated schematically in fig. 27, which shows the time average of some dependent variable of the system versus p (cf. fig. 4 of ref. 17 and fig. 1 of Ref. 18. For $p_a > p > p_1$ both attractors occur simultaneously with different basins of attraction. In the

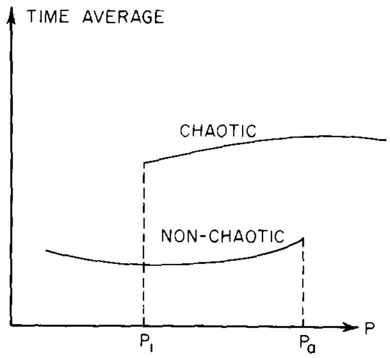

Fig. 27. Schematic illustration of the time average of a dependent variable versus a parameter p.

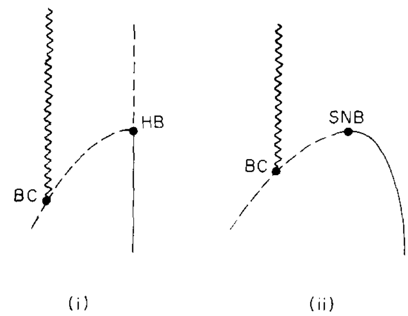

Fig. 28. (i) Crisis diagram for the Lorenz attractor case and (ii) for cases (b) and (c) of the text. BC, HB, and SNB denote boundary crisis, inverted Hopf bifurcation and saddle node bifurcation of periodic orbits.

case of the Lorenz attractor the non-chaotic attractor is a fixed point, while for cases (b) and (c) the non-chaotic attractors are limit cycles. As p is increased past p_a the non-chaotic attractors are destroyed by bifurcations. For the Lorenz case the bifurcation is of the inverse Hopf type. Namely, for $p < p_a$ an unstable limit cycle exists, which, as p approaches p_a, collapses to the stable fixed point, converting it to an unstable fixed point for $p > p_a$. For cases (b) and (c), we beliefe that the bifurcation is of the saddle-node type. That is, for $p < p_a$ an unstable (saddle) limit cycle again exists; as p approaches p_a the attracting stable limit cycle (node) and the unstable limit cycle coalesce and annihilate each other. Thus in all cases an unstable periodic orbit exists in the range $p_a > p > p_l$. The stable manifold of this unstable periodic orbit forms the boundary separating the basins of attraction of the chaotic and non-chaotic attractors. As p decreases toward p_l, the chaotic attractor moves closer to the unstable orbit on the boundary, until, at $p = p_l$, a crisis occurs. If one examined the surface of section, the situation would be similar to that illustrated in fig. 12 for the boundary crises for the Hénon map. Fig. 28 gives a crisis diagram summarizing the sequence of events for the three cases (p increases vertically) [19]. Furthermore, Yorke and Yorke [10] have numerically reduced the Lorenz system of equations to a one-dimensional map and have used this to examine the statistical characteristics of the resulting chaotic transients and their dependence on a system parameter. Their work also confirms the existence of an exponential distribution of lifetimes for these transients.

5. Fractal torus crises

Here we wish to consider a particular type of crisis which occurs only in invertible maps whose dimension is at least three. Our discussion will be brief, with further results and details to be given in a future publication [20]. To begin, we consider a bifurcation of a three-dimensional map in which two unstable fixed points, R and A, are created as a parameter δ decreases through one (cf. fig. 29). The fixed point R has one stable direction (s in fig. 29) and two unstable directions (u and ξ in fig. 29), while A has two stable directions (s and ξ) and one unstable direction (u). When R and A are close together (δ slightly less than one), we represent the map locally in the region near R and A as $u_{n+1} = \lambda_u u_n$, $s_{n+1} = \lambda_s s_n$, $\xi_{n+1} = \xi_n^2 + \delta/2$, where $\lambda_u > 1 > \lambda_s > 0$. The two fixed points of this map corresponding to R and A for $1 > \delta > 0$ are $u = s = 0$ and $\xi = 1 \pm (1-\delta)^{1/2}$. As δ increases toward one, R and A move toward each other and coalesce at $\delta = 1$. For $\delta > 1$, the two fixed points no longer exist.

The local picture just given is elementary. However, the global consequences of this bifurcation

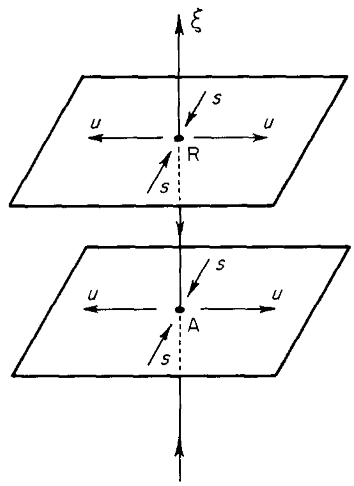

Fig. 29. Local illustration of an unstable pair of fixed points.

are not so clear. In particular, we suggest the possibility that the closure of the unstable manifold emanating from A forms a chaotic attractor. Similarly, since time reversal interchanges the roles of R and A, we also consider the possibility that the closure of the stable manifold emanating from R is a chaotic repellor (i.e. it is a chaotic attractor on time reversal). Furthermore, it seems reasonable from fig. 29 that this repellor might form the boundary of the basin of attraction for the strange attractor. If the set of hypotheses just given do in fact occur, and the point A is in the strange attractor, then when A coalesces with R we expect that the strange attractor will be destroyed. Since R is on the boundary of the basin of attraction, the destruction of the attractor is due to a boundary crisis.

To demonstrate that this picture can in fact occur, it suffices to give an example. The example which we choose is a modification of a map previously studied in ref. 21,

$$x_{n+1} = (x_n + y_n) \mod 1, \tag{6a}$$

$$y_{n+1} = (x_n + 2y_n) \mod 1, \tag{6b}$$

$$z_{n+1} = \lambda z_n + z_n^2 + \epsilon \cos(2\pi x_n), \tag{6c}$$

where we assume $\epsilon, \lambda > 0$. Below, we shall demonstrate numerically that this example does, in fact, yield an attractor with the required behavior. Even so, the example appears to be a very special one; e.g., the x and y equations do not depend on z and are area preserving (in fact, the x–y component of the map is the well-known "cat map" of Arnol'd). Thus, even if this map demonstrates the phenomena, one might still question whether these phenomena are to be expected in typical dynamical systems. To answer this question we have numerically studied the stability of our qualitative results under perturbations. That is, we have added to the x, y and z equations perturbing functions of x, y and z which are of a fairly arbitrary nature. We find that the qualitative results appear to survive these perturbations (cf. ref. 20), and thus we believe that our picture should be added to the list of events possible in typical dynamical systems.

For the map (6) we may think of x and y as angle coordinates (due to the mod 1) and z as a radial coordinate. Thus we are essentially dealing with a toroidal coordinate system. We note that the system (6) has a pair of fixed points at $x = y = 0$, $z = z_{\mathrm{R,A}} = \frac{1}{2}\{(1-\lambda) \pm [(1-\lambda)^2 - 4\epsilon]^{1/2}\}$, corresponding to R and A of fig. 29. Since the term $\cos(2\pi x)$ in (6b) is maximum at the fixed point (i.e., at $x = 0$), we expect that the attractor will assume its maximum z-value at this fixed point. Similarly, the repellor will assume its minimum z-value at this fixed point. Thus, if the two touch, they will first do so at $x = y = 0$, and the attractor will cease to exist after this happens. From the expression for $z_{\mathrm{R,A}}$ we see that the strange attractor is expected to exist for $\lambda \leqslant \lambda_c \equiv 1 - 2\epsilon^{1/2}$ with a crisis occurring at $\lambda = \lambda_c$. Fig. 30 shows a $y = 0$ cross-section of the attractor (inner curve) and the encircling repellor for eqs. (6) obtained by numerical iteration with $\epsilon = 0.04$ and $\lambda = 0.58 < \lambda_c = 0.60$. For the attractor, the cross-section is obtained by numerically iterating eqs. (6), and, after transients have died away, plotting points whose y-values lie between $y = \pm 10^{-3}$. The repellor curve is obtained similarly by iteration of the inverse map (to do this one must choose the plus sign when inverting the quadratic z equation). The z and x values in this

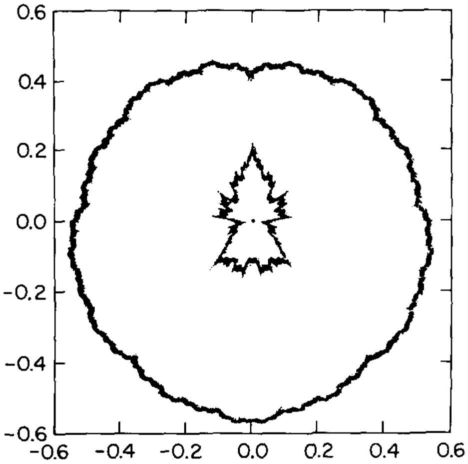

Fig. 30. $y = 0$ cross-section of the attractor and its basin boundary for eq. (6) with $\lambda = 0.58$ and $\epsilon = 0.04$.

figure have been plotted in polar coordinates to emphasize that what is shown represents cross-sections of toroidal surfaces. The origin of the polar coordinate system is signified by a dot on the figure; $2\pi x$ represents the polar angle from the vertical; and $z + 0.1$ is the radial distance from the origin. The cross-section of both the attractor and the repellor appear to be fractal curves which are continuous but nowhere differentiable. Orbits initialized at radial positions falling within the region bounded by the repellor are observed to be attracted to the attractor, while those initialized outside this region are observed to approach $z = \infty$ as

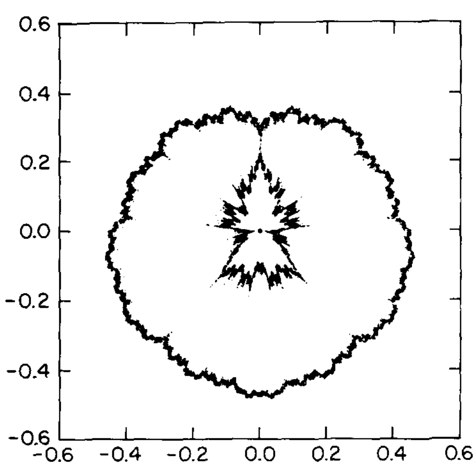

Fig. 31. Same as in fig. 30 but $\lambda = 0.68$.

$n \to \infty$. Thus the repellor surface is the boundary of the basin of attraction for the attractor. As λ is raised the z-coordinates at $x = y = 0$ of the repellor and attractor appear to move towards each other. After the crisis occurs, the attractor and repellor remnants are still visible on our plots because the chaotic transients can be quite long. Fig. 31 shows such a plot for $\epsilon = 0.04$ and $\lambda = 0.68 > \lambda_c$. Note the apparent joining of the attractor and repellor at $x = 0$.

6. Conclusions

In this paper we have illustrated crisis phenomena for chaotic attractors in a one-dimensional noninvertible map, a two-dimensional invertible map, three-dimensional flows, and three-dimensional maps. Our results show that crises are prevalent in many circumstances and systems and serve to illustrate their accompanying characteristic statistical behavior (e.g., chaotic transients). Based on these results, we are lead to propose the following two conjectures:

1) Almost all sudden changes in the size of chaotic attractors are due to crises.
2) Almost all sudden creations and destructions of chaotic attractors with their basins are due to crises.

For the purposes of these conjectures, and depending on the results of future research, it may be that the definition of a crisis (section 1) should be widened to include collisions of chaotic attractors with either unstable fixed points, unstable periodic orbits or unstable *multiply* periodic orbits (i.e. tori).

Note that conjecture 2 is not violated, for example, by the existence of a tangent bifurcation transition from a chaotic to a non-chaotic orbit (see, for example, fig. 2), because the attractor basin is neigher created nor destroyed in such a transition. Thus a single identifiable attractor remains throughout the transition but changes its character (subduction).

Also note in the statements of these conjectures the phrase "almost all". By this we mean to indicate that there may be special examples of dynamical systems which violate our conjectures, but which we believe are atypical in the sense that arbitrarily small perturbations of these systems restore the validity of our conjectures.

In conclusion, we wish to emphasize that the study of sudden changes in chaotic dynamics is just at its beginning, and that we believe that many new and intriguing phenomena await discovery. This will be particularly so as phenomena in higher dimensions begin to be explored (cf., for example, our section 5).

Acknowledgements

This work was supported by the Office of Basic Energy Sciences of the U.S. Department of Energy under contract No. DE-AS05-82ER-12026. One of us (J.A.Y.) was also partly supported by AFOSR, Air Force Systems Command under Grant No. AF0FR-81-0217A.

References

[1] J.E. Marsden and M. McCracken, The Hopf Bifurcation and Its Applications (Springer, Berlin, 1976). D. Ruelle and F. Takens, Comm. Math. Phys. 20 (1971) 167.

[2] M.J. Feigenbaum, J. Stat. Phys. 19 (1978) 25. P. Collet and J.-P. Eckmann, Iterated Maps on the Interval as Dynamical Systems (Birkhauser, Boston, 1980). R.M. May, Nature 261 (1976) 459. E. Ott, Rev. Mod. Phys. 53 (1981) 655. J.-P. Eckmann [7].

[3] C. Grebogi, E. Ott and J.A. Yorke, Phys. Rev. Lett. 48 (1982) 1507.

[4] S.-J. Chang and J. Wright, Phys. Rev. A 23 (1981) 1419.

[5] C. Simo', J. Stat. Phys. 21 (1979) 465.

[6] J.L. Kaplan and J.A. Yorke, Comm. Math. Phys. 67 (1979) 93.

[7] J.-P. Eckmann, Rev. Mod. Phys. 53 (1981) 643.

[8] G. Pianigiani and J.A. Yorke, Trans. Amer. Math. Soc. 252 (1979) 351. A. Lasota and J.A. Yorke, Rend. Sem. Univ. Padova 64 (1981) 141.

[9] G. Pianigiani, J. Math. Anal. Appl., in press.

[10] J.A. Yorke and E.D. Yorke, J. Stat. Phys. 21 (1979) 263.

[11] J. Guckenheimer, Comm. Math. Phys. 70 (1979) 133. I. Gumowski and C. Mira, Recurrences and Discrete Dynamic Systems (Springer-Verlag, New York, 1980).

[12] Y. Pomeau and P. Manneville, Comm. Math. Phys. 74 (1980) 189.

[13] S. Newhouse, Publ. Math. IHES 50 (1980) 101.

[14] S. Smale, Bull. Am. Math. Soc. 73 (1967) 747. Y. Treve, Topics in Nonlinear Dynamics (Am. Inst. Physics, New York, 1978) p. 147.

[15] J. Testa, J. Perez and C. Jeffries, Phys. Rev. Lett. 48 (1982) 714; C. Jeffries and J. Perez, Phys. Rev. A27 (1983) 601.

[16] E.N. Lorenz, J. Atmos. Sci. 20 (1963) 130.

[17] D.A. Russell and E. Ott, Phys. Fluids 24 (1981) 1976.

[18] B.A. Huberman and J.P. Crutchfield, Phys. Rev. Lett. 43 (1979) 1743.

[19] See also the paper of C. Tresser, P. Coullet and A. Arneodo [J. Physique-Lett. 41 (1980) L-243] for a discussion of discontinuous transitions to chaos involving hysteresis as in figs. 27 and 28.

[20] C. Grebogi, E. Ott and J.A. Yorke, to be published.

[21] J.L. Kaplan, J. Mallet-Paret and J.A. Yorke, to be published.